*American Mineralogist, Volume 102, pages 85–91, 2017*

SPECIAL COLLECTION: APATITE: A COMMON MINERAL, UNCOMMONLY VERSATILE

# Raman and IR studies of the effect of Fe substitution in hydroxyapatites and deuterated hydroxyapatite

**Anastasios Antonakos[1], Efthymios Liarokapis[1,*], Andreas Kyriacou[2], and Theodora Leventouri[2]**

[1]Department of Physics, National Technical University of Athens, 15780 Athens, Greece
[2]Physics Department, Florida Atlantic University, Boca Raton, Florida 33431, U.S.A.

## Abstract

We have studied synthetic Fe-substituted hydroxyapatite $Ca_{5-x}Fe_x(PO_4)_3OH$ and the corresponding deuterated samples with varying Fe concentrations $x$ ($0 \le x \le 0.3$) by Raman and IR spectroscopy at room temperature. In the IR spectra, substitution of deuterons for protons affects the OH internal mode in a way consistent with the mass difference of the substituting ions, as well as a mode attributed to vibrations of the $Ca_3$-(OH) unit. In the Raman spectra, the frequency of all modes is not noticeably affected by the Fe substitution. Raman bands show increased width and substantial reduction in intensity with increasing amount of Fe, presumably related to disorder introduced by the substitution. We find that the disorder is smaller in the hydroxyapatites compared to the deuterated ones.

**Keywords:** Hydroxyapatites, Fe-substitution, Raman spectroscopy, FTIR

## Introduction

Iron is a biologically important trace element substituting for Ca in the hydroxyapatite (HAp) structure (0.003 wt% in enamel, 0.01–0.1 wt% in bone). It has been demonstrated that Fe-deficient rat bones exhibit decreased mechanical strength, decreased bone mass density, and increased fragility (Medeiros et al. 2002), whereas Fe overload leads to decreased osteoblast cell number and activity (De Vernejoul et al. 1984). Disagreements on the structural modifications and related properties that the Fe for Ca substitution causes in the apatite lattice are reported in the literature (Wu et al. 2007; Low et al. 2008; Khudolozhkin et al. 1974; Morissay et al. 2005; Jiang et al. 2002; Li et al. 2012; Salviulo et al. 2011). In a recent publication we have shown that Fe substitutes at both Ca(1) and Ca(2) crystallographic sites with a preference at the Ca(2) site by applying simultaneous Rietveld refinement of X-ray diffraction (XRD) and neutron powder diffraction (NPD) powder patterns of Fe-substituted, deuterated (FeDAp) powder samples (Kyriacou et al. 2013).

Here we present Raman and FTIR studies of the same series of FeHAp and FeDAp powder samples. We have studied the effect of the deuteron substitution for H on certain modes and compared experimental results with first-principles calculations (Corno et al. 2006; Pedone et al. 2007; Calderin et al. 2005; Ulian et al. 2013). Our results indicate that Fe substitution strongly affects the intensity of the internal modes of the $PO_4$ tetrahedra, due to the lattice distortion introduced by Fe at the Ca sites. Furthermore, it is found that the disorder in the lattice of deuterated hydroxyapatites is more sensitive to the Fe substitution.

## Experimental methods

The powder compounds studied have the chemical form $Ca_{5-x}Fe_x(PO_4)_3OH$ (FeHAp) with Fe atomic concentration $0 \le x \le 0.3$). A similar set had been deuterated in flowing oxygen-enriched $D_2O$ at 600 °C (FeDAp). Table 1 lists the composition of the investigated samples. A 0.2 M solution of $Ca(NO_3)_2{\cdot}4H_2O$ (99.98% ALPHA AESAR) was added drop wise to a 0.12 M solution of $(NH_4)_2PO_4{\cdot}4H_2O$ (99.99% ALDRICH) at ambient conditions. The pH was maintained at 9.5 ± 0.1 by adding $NH_4OH$. Hydroxyapatite was formed according to the reaction:

$$5Ca(NO_3)_2 + 3(NH_4)_2HPO_4 \xrightarrow{NH_4OH} Ca_5(PO_4)_3OH.$$

Then, $FeCl_2{\cdot}4H_2O$ solution, heated to 85 °C, was added drop wise to the HAp solution. Fe-substituted HAp formed according to the reaction:

$$Ca_5(PO_4)_3OH + xFeCl_2 \rightarrow Ca_{5-x}Fe_x(PO_4)_3OH.$$

The final precipitate was aged for 20 h, washed, dried, and heat-treated in a tube furnace at 650 °C for 15 h under flowing $N_2$ to prevent oxidation of the Fe ions.

Detailed information on the preparation conditions and characterization from simultaneous Rietveld refinements of X-ray and neutron powder diffraction, X-ray diffraction (XRD) and neutron powder diffraction (NPD), transmitted electron microscopy (TEM), and magnetometry methods has been published elsewhere (Kyriacou et al. 2013). A mixture of irregularly shaped rods and spherical particles with dimensions between 15 and 65 nm was observed in the TEM image of FeHAp0, while the size range is limited to 20 to 50 nm in the FeDAp0 sample. When Fe substitutes for Ca, the size range and shapes of the samples remain unaltered regardless of the Fe concentration $x$.

Micro-Raman spectra were obtained at room temperature using a T64000 Jobin-Yvon triple spectrometer, equipped with a liquid nitrogen cooled Charge Coupled Device (CCD) and a microscope. The 514.5 nm wavelength of an $Ar^+$ laser was used for excitation in a backscattering geometry of the sample under the microscope. The spectrum accumulation time was 3 h and the laser power at the sample was 0.2 mW. The spectrometer was calibrated before and after each measurement using a silicon wafer or a reference Kr lamp. Because of the random orientation of the microcrystals in the powder samples, no exact selection rules could be applied. The selection rules could give only limited information about the properties of the Raman tensors because of the random orientation of the microcrystallites in the powder samples. The differentiation of orientation was studied by turning the sample stage between 0° to 90° while no dependence was found by changing the polarization of the laser. Therefore, the spectra of all samples were recorded with random polarization. The 100× (N.A. 0.95) and 50× (N.A. 0.80) magnification

* E-mail: eliaro@central.ntua.gr
Special collection papers can be found online at http://www.minsocam.org/MSA/AmMin/special-collections.html.

0003-004X/17/0001–085$05.00/DOI: http://dx.doi.org/10.2138/am-2017-5884

lenses were employed for the Raman measurements with the laser spot focused to ~1 and ~2 μm, respectively. Theoretically one would expect a 20% larger spot for the 50× magnification and roughly two times larger confocal volume. The confocal configuration of the spectrometer, together with the micrometric probe size, reduces the fluorescence problems encountered in the conventional Raman spectroscopy of such materials (Penel et al. 1998; Okazaki and Takahashi 1997; Wopenka and Pasteris 2005).

The Fourier transform infrared (FTIR) spectra were recorded using a Bruker Optic IFS66v/S interferometer equipped with a MIRacle Single Reflection Attenuated Total Reflectance (ATR) unit with a diamond/ZnSe crystal plate. The range of frequencies was 525–4000 $cm^{-1}$, and the spectra were recorded at ambient conditions with a resolution of 2 $cm^{-1}$. To obtain a good signal-to-noise ratio, 1200 scans were collected and averaged. A KBr beam splitter was used for the M-IR source. The ATR unit permits spectra collection without any specific sample preparation, but only for the region above 525 $cm^{-1}$. A high-pressure lamp has been used to achieve high spectral quality and to avoid low-pressure effects. Since the pressure effect of the ATR accessory could not be measured, an empirical method was used whereby the variations of intensities and the ratio of the intensities were considered as a function of pressure; they increase to a maximum and then remain fairly constant as the applied force is increased further.

## Results and discussion

Figure 1a presents the ATR FTIR spectra of all samples in the high frequency region. The continuous line spectra correspond to the as prepared FeHAp samples, and the dotted ones to the deuterated FeDAp samples. The sharp band at ~3572 $cm^{-1}$ in the FeHAp spectra for all Fe concentrations is assigned to the OH stretching mode (Elliott 1994, and references therein). The mode frequency is mostly related to the mass of the H and therefore, D substitution for H should modify its frequency mainly according to the mass ratio of the two H isotopes. The absence of this mode from the FeDAps and the appearance of a sharp band at ~2633 $cm^{-1}$ confirms the deuteration of the samples. In particular, the frequency of this band follows approximately the mass rule

$$\omega_{D-O} = \omega_{H-O} (M_{D-O}/M_{H-O})^{1/2}.$$

Figure 1b shows the lower frequency part of the ATR FTIR spectra of all samples. Several peaks appear, located at ~566, 600, 631, 963, 1026, and ~1088 $cm^{-1}$. Of these modes, only that at ~631 is affected by the deuteron substitution, while the remainder are not noticeably modified. Some small changes in frequency of the ~1026 $cm^{-1}$ peak are most likely due to intensity modifications of those modes that contribute to this peak. The first two modes at ~566 and ~600 $cm^{-1}$ have been attributed to the $\nu_4$ doubly degenerate asymmetric O-P-O bending mode of the $PO_4$ tetrahedron (Antonakos et al. 2007, and references therein). The higher frequency peaks at 1026, and ~1088 $cm^{-1}$ are related to the $\nu_3$ triply

**Table 1.** Samples studied, corresponding phase identification, and identified phases (from Kyriakou et el. 2013)

| File names of hydroxyapatite | Chemical formula | File names of deuterated apatites | Nominal Fe content *x* | Identified impurity phases (from Kyriakou et el. 2013) |
|---|---|---|---|---|
| FeHAp0 | $Ca_5(PO_4)_3OH$ | FeDAp0 | 0.00 | |
| FeHAp005 | $Ca_{4.95}Fe_{0.05}(PO_4)_3OH$ | FeDAp005 | 0.05 | |
| FeHAp01 | $Ca_{4.90}Fe_{0.10}(PO_4)_3OH$ | FeDAp01 | 0.10 | |
| FeHAp02 | $Ca_{4.80}Fe_{0.20}(PO_4)_3OH$ | FeDAp02 | 0.20 | $\alpha$-$Fe_2O_3$ |
| FeHAp03 | $Ca_{4.70}Fe_{0.30}(PO_4)_3OH$ | FeDAp03 | 0.30 | $\alpha$-$Fe_2O_3$ |

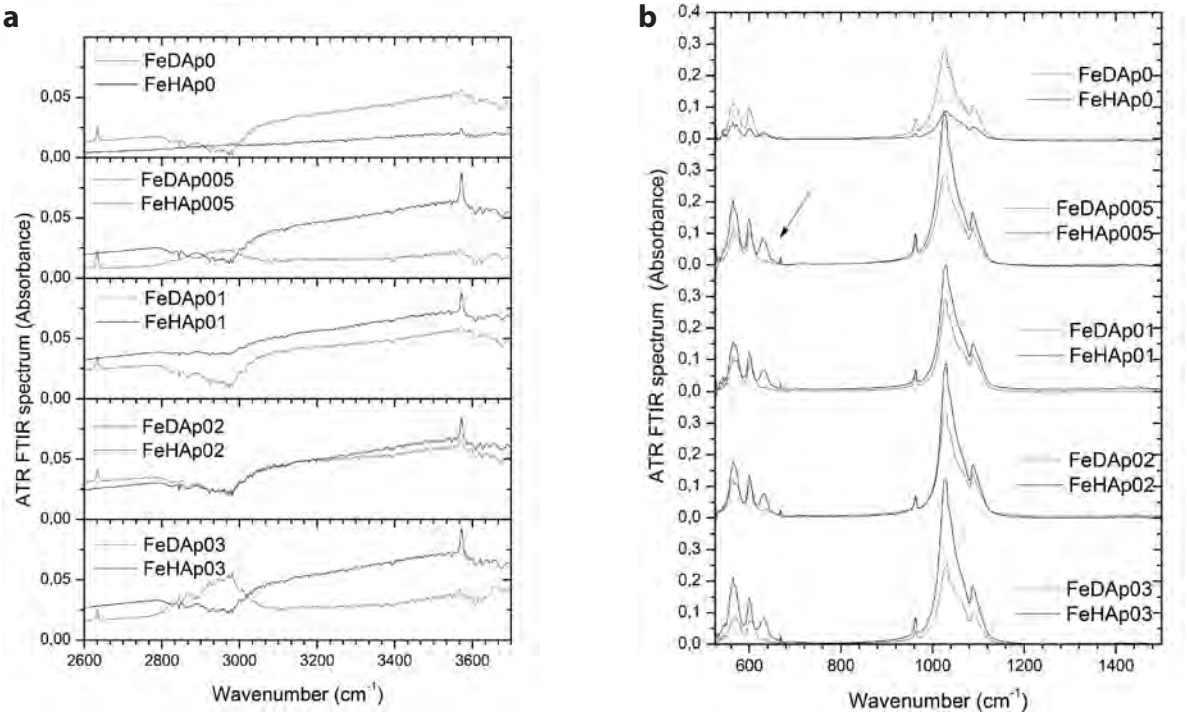


**Figure 1.** IR spectra of iron-doped hydroxyapatites (continuous lines) and deuterated oxypatites (dotted lines) for all samples in the high- (**a**) and low- (**b**) frequency spectral region. The arrow in **b** indicates the mode that disappears with deuteration.

degenerate asymmetric P-O stretching mode of the $PO_4$ tetrahedron (Antonakos et al. 2007, and references therein). The weak but sharp band at 963 $cm^{-1}$ can be assigned to the $\nu_1$ vibration (symmetric P-O stretching mode) of the $PO_4$ tetrahedron (Penel et al. 1998; Antonakos et al. 2007; Park et al. 2002). Finally, the weak mode at ~631 $cm^{-1}$ has been attributed to the OH librational mode of the Ca3-OH group, i.e., the OH ion straddles across the Ca triangles that are situated on the mirror plane of the apatite structure (Cant et al. 1971; Elliott 1994; Antonakos et al. 2007). Some ab initio calculations assign this mode to the internal $\nu_4$ vibrations (Corno et al. 2006; Pedone et al. 2007). This does not appear to be correct, since this mode disappears almost completely on deuteration, and is neither affected in intensity nor width by the Fe substitution. As we will see below in the Raman spectra, Fe substitution reduces substantially the intensity and increases the width of the internal vibration modes of the $PO_4$ tetrahedron. Therefore, the mode must be related to the OH librational vibration of the $Ca_3$-(OH) group. Unfortunately, ATR did not allow lower frequency measurements to follow the mode in the expected frequency from the mass difference H-D. Table 2 presents the detected IR and Raman modes and their assignment (Elliott 1994; Antonakos et al. 2007).

Figure 2 presents data with 100× (dotted line) and 50× (continuous line) magnifications for the low- (Fig. 2a) and high- (Fig. 2b) frequency regions. Although in our previous investigations of apatite higher magnification gave stronger peaks (Antonakos et al. 2007), this did not occur in this study, presumably due to the diffused light by the nanostructured samples that favors the longer focusing. Several peaks can be discriminated mainly with the 50× magnification. In the low frequency part (Fig. 2a) these are located at ~330 $cm^{-1}$ (very weak) and ~431, 448, 581, 593, 610, and ~617 $cm^{-1}$ (strong ones). The two strong ones at ~431 and ~448 $cm^{-1}$ have been assigned to $\nu_2$ vibrations, while the other four modes at higher frequency belong to the $\nu_4$ mode of the $PO_4$ group. The origin of the weak mode at ~330 $cm^{-1}$ will be discussed below. In the high-frequency region (Fig. 2b) the peaks are located at ~839, 894, 916, 925, 962, 1027, 1040, 1046, 1075, 1122, 1252, and 1297 $cm^{-1}$. Most of them can be only observed with the 50× magnification. From those peaks, the ones at ~1027, 1040, 1046, and ~1075 $cm^{-1}$ have been assigned by several authors to the $\nu_3$ vibrations, and the one at ~962 $cm^{-1}$ to $\nu_1$ of the $PO_4$ unit (Antonakos et al. 2007). The lower frequency modes (843–925 $cm^{-1}$) are related neither to Fe introduced to the sample nor to an Fe oxide impurity since they are not modified in intensity by increasing the amount of Fe. Modes at relative frequencies have been proposed in shell model lattice dynamic calculations (Calderin et al. 2005), but other more recent theoretical calculations did not find any modes related to the undoped HAp in this frequency region (Corno et al. 2006; Pedone et al. 2007; Ulian et al. 2013). Most likely the bands at 843 and 894 $cm^{-1}$ are related to atmospheric $CO_3^{2-}$ ions entering the HAp structure during the sample preparation. Similar results were obtained in other studies (Leventouri et al. 2003; Antonakos et al. 2007). Then the two broad bands at ~1252 and ~1297 $cm^{-1}$ are related to $CO_3^{2-}$/amide and/or $HPO_4^{2-}$ impurities

**TABLE 2.** Raman and IR modes and their assignments

| Mode frequency ($cm^{-1}$) | Detected in the compounds | Spectroscopic method | Assignment (Elliott 1994; Antonakos et al. 2007) |
|---|---|---|---|
| 223, 244, 291, 409, 612, 1320 | all with Fe, increase with Fe | Raman | $\alpha$-$Fe_2O_3$ (hematite) |
| 839, 894, 916, 925 | all | Raman | $\nu_4$ $CO_3$ and/or $HPO_4^{2-}$ impurities |
| 566, 600 | all | IR | $\nu_4$ $PO_4$ |
| 631 | FeHAp | IR | $Ca_3$-(OH) librational OH mode |
| 963 | | IR | $\nu_1$ $PO_4$ |
| 1026, 1088 | all | IR | $\nu_3$ $PO_4$ |
| 2633 | FeDAp | IR | OH |
| 3572 | FeHAp | IR | OH |
| 330 (very weak) | Dap, HAp | Raman | $Ca_3$-(OH)? |
| 431, 448 | all, decrease with Fe content | Raman | $\nu_2$ $PO_4$ |
| 581, 593, 610, 617 | all, decrease with Fe content | Raman | $\nu_4$ $PO_4$ |
| 962 | all, decrease with Fe content | Raman | $\nu_1$ $PO_4$ |
| 1027, 1040, 1046, 1075 | all, decrease with Fe content | Raman | $\nu_3$ $PO_4$ |
| 1252, 1297 | all | Raman | $CO_3$, amide and/or $HPO_4^{2-}$ impurities |

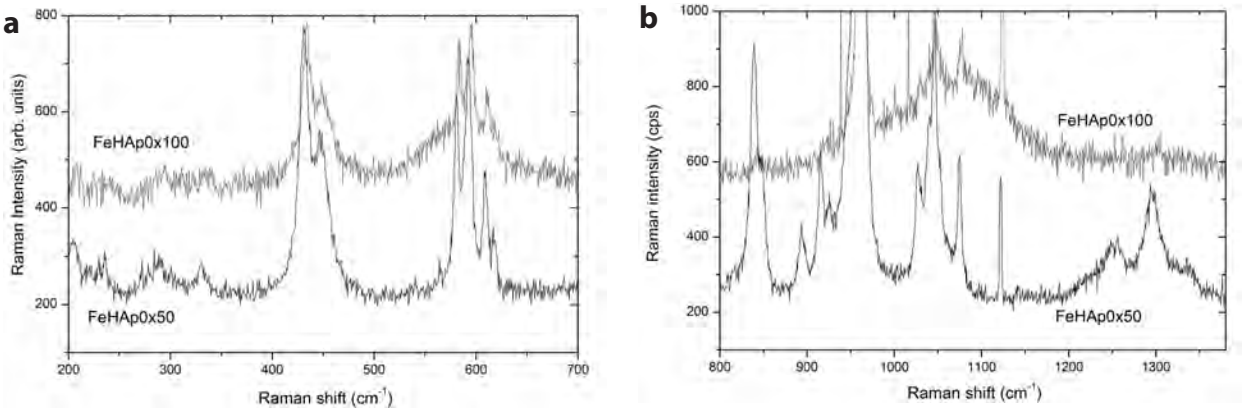


**FIGURE 2.** Raman spectra of the low- (**a**) and high- (**b**) frequency regions of the $x = 0.0$ hydroxyapatite sample with 100× (dotted line) and 50× (continuous line) magnification.

(Vignoles-Montrejaud 1984; Penel et al. 1998; Antonakos et al. 2007). Finally, the very narrow band at ~1122 $cm^{-1}$ is a signal from the fluorescence lamp.

Figure 3 shows the effect of the 0.30 atomic nominal Fe substitution for Ca corresponding to the two magnifications. In the low-frequency region (Fig. 3a) all strong modes that appear in the pure HAp spectrum completely disappear, while new peaks appear located at ~224, 244, 291, 409, and ~498 $cm^{-1}$. All of them belong to hematite (de Faria et al. 1997). A peak at ~612 $cm^{-1}$ is mainly from the strong hematite band, which masks the narrow weaker $\nu_4$ $PO_4$ peaks of the HAp (seen in Fig. 2a). The lower frequency part of Figure 3b (843–925 $cm^{-1}$) and the $\nu_1$ $PO_4$ mode remain practically unchanged in intensity. The $\nu_3$ $PO_4$ modes are damped and broaden due to disorder introduced by the Fe substitution. The $\nu_3$ $PO_4$ region was found in previous studies to be very sensitive upon substitution due to the different HAp environments present (Elliott 1994; Penel et al. 1998; Antonakos et al. 2007). At higher frequency, a new strong broad band develops upon Fe substitution at 1320 $cm^{-1}$. This band is expected to appear strong when excited with the 514 nm laser and is related to $\alpha$-$Fe_2O_3$ (hematite) (Wang et al. 2005). Although this band was observed previously, the explanation for the wavelength response behavior and for its origin is still unclear, and may be caused by a two magnon scattering process (Martin et al. 1977) or a resonance-enhanced two-phonon scattering process (McCarty 1988; Massey et al. 1990; Shim and Duffy 2001). The fundamental mode could be the 660 $cm^{-1}$ IR active Eu band of hematite and therefore an overtone.

The evolution of the Raman spectra with increasing Fe substitution is presented in Figure 4a for the low-frequency part of FeDAps. It is observed that the intensity of the modes assigned to hematite (marked by straight lines) increase with the amount of Fe substitution, as presented in Figure 4b. On the one hand, XRD results have detected traces of increasing amounts of hematite starting from the x = 0.20 nominal atomic substitution (Kyriacou et al. 2013). On the other hand, Raman spectroscopy that is more sensitive to detect impurities, indicates that the hematite

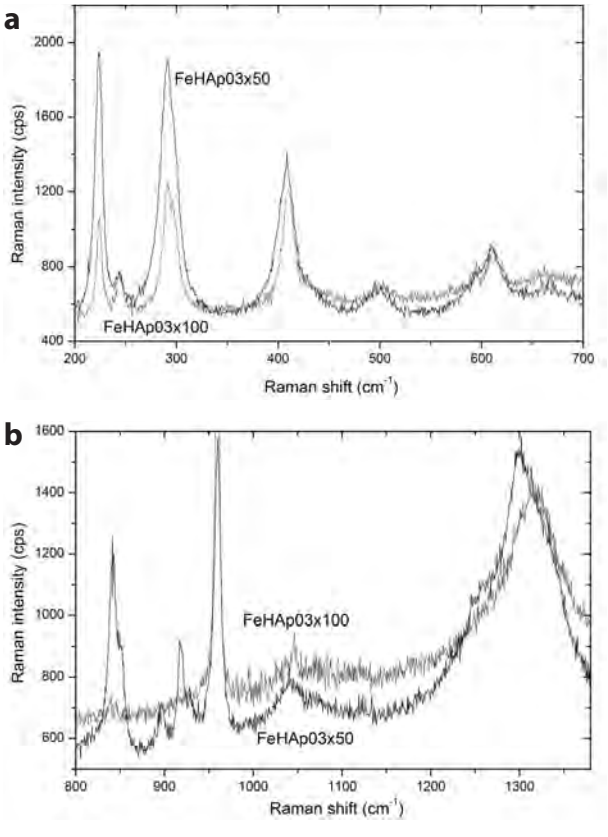


**Figure 3.** Raman spectra of the low- (**a**) and high- (**b**) frequency regions of the Fe-doped ($x$ = 0.3) hydroxyapatite sample with 100× (dotted line) and 50× (continuous line) magnification.

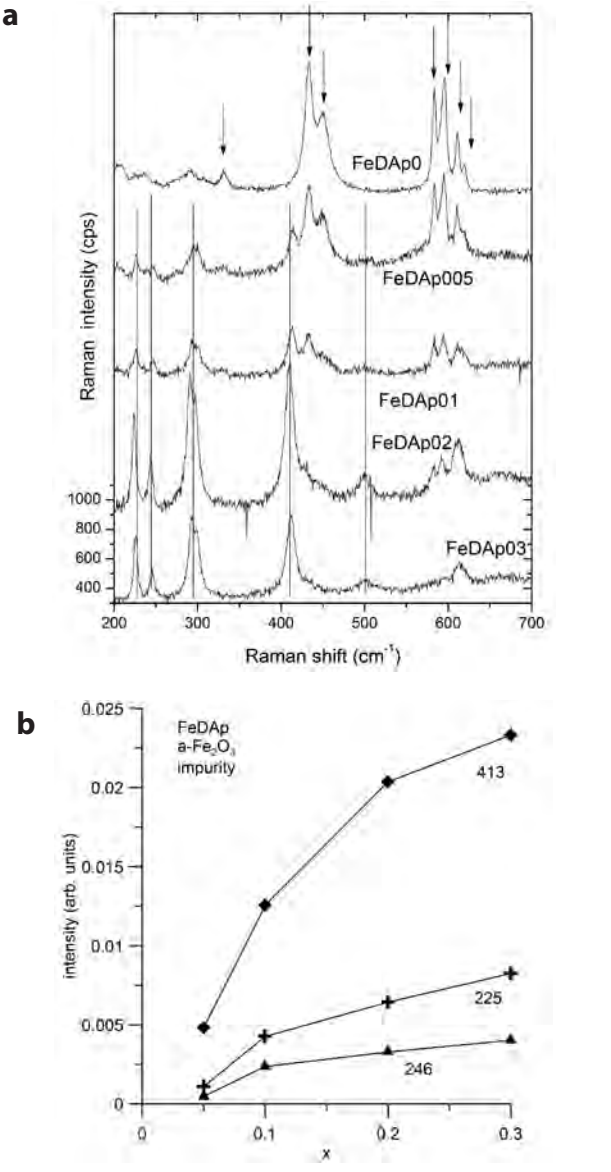


**Figure 4.** (**a**) Raman spectra of the FeDAp samples (low-frequency region). Straight lines indicate the peaks due to the $\alpha$-$Fe_2O_3$ phase and arrows the Raman modes of the apatite. (**b**) The dependence on the Fe nominal atomic substitution of the new modes attributed to the hematite phase.

phase is present in all Fe substituted compounds, even for x = 0.05 (Fig. 4b). The intensity of the modes assigned to internal vibrations of the $PO_4$ tetrahedra (marked by arrows) continuously decreases with increasing amounts of Fe, and almost completely disappears for the 0.02 atomic nominal Fe substitution for Ca. The comparison of Figure 2a (x = 0) with Figure 3a (x = 0.3) shows that the effect is similar for the as-prepared set of samples (FeHAp). In the low-frequency region of the Raman spectra, a mode of E1 symmetry related to Ca-OH is expected at 330 $cm^{-1}$ (Pedone et al. 2007). A mode at close frequency (332 $cm^{-1}$) is observed in pure DAp, which gradually disappears with Fe substitution (Fig. 4a). This mode involves vibrations of OH. Therefore, the D substitution would affect (decrease) its frequency. In Figure 2a (HAp), this mode appears unshifted at the same frequency, hence, questioning its assignment to vibrations that involve the OH units (Pedone et al. 2007).

The Fe substitution for Ca could introduce disorder by the breaking of long-range symmetry and shifting to lower frequencies of the modes involving the Ca atoms owing to their mass difference. The internal modes of the $PO_4$ units should not be affected significantly. Except from a substantial reduction in intensity (Fig. 4a), the internal modes are not modified in frequency, probably because of the only small amounts of Fe (up to 0.3 atomic, nominal content).

Depending on the mass difference between the substituting (Fe) and the original (Ca) atom, the compound could follow one or two mode behaviors (Srivastava 1990). In the former case, there will be a gradual shift in frequency toward the limiting value of a hypothetical system with 100% Fe at the Ca site. In the latter, there will be a gradual development of another mode that will correspond to the frequency of the hypothetical end-member. Due to the different coordination of the substituting Fe, it is very unlikely to assume one-mode behavior, since the internal modes of $PO_4$ will be affected only indirectly by the breaking of the external bonds to the Ca sites. Concerning the effect of the mass difference between Fe and Ca on the vibrational modes, ab initio calculations have investigated $^{42}Ca$ isotopic substitution for $^{40}Ca$ (5% mass difference at the Ca sites) and deuteration (Corno et al. 2006). It has been found (Corno et al. 2006), that the expected frequency shifts for modes above ~600 $cm^{-1}$ will not exceed ~1 $cm^{-1}$. Only Raman bands of frequency less than ~400 $cm^{-1}$ are expected to be shifted by a few $cm^{-1}$ (Corno et al. 2006). In our case, even for x = 0.30 (6% atomic Fe substitution for Ca) there will only be a 2.5% mass difference with the partial substitution of Fe for Ca. Therefore, the mass effect on the vibration frequencies will be even smaller. Concerning deuteration, only peaks in the range ~600 $cm^{-1}$ are expected to be shifted substantially (Corno et al. 2006). From the observed modes in both IR and Raman spectra, only the above-mentioned mode at ~631 $cm^{-1}$ is affected, but, as previously discussed, should be correlated to an OH vibrational mode and not a $PO_4$ one (Fig. 1b). The rest of the modes appear at the same frequency in both HAp and DAp (Figs. 1b, 2, and 4a).

What is impressive is the strong reduction in intensity of the majority of the modes in the Raman spectra (Figs. 4a and 5) even with such small amounts of Fe substitution (maximum nominal atomic amount 6%). As found by Kyriacou et al. (2013), $Fe^{3+}$ appears in a fourfold coordination, breaking some bonds with

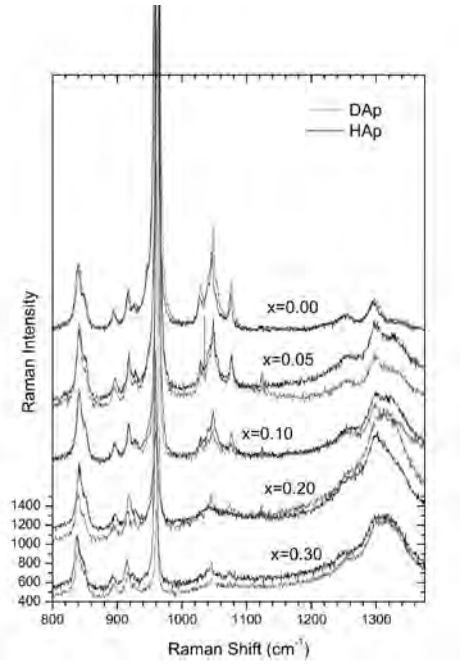


**FIGURE 5.** Raman spectra of FeHAp (continuous lines) and FeDAp (dotted lines) for all Fe concentrations. All spectra have the same scale presented on the vertical axis.

the O(2) and O(3) nearest neighbors, while $Fe^{2+}$ is in a sixfold coordination breaking the bond with O(1). The difference in mass between the two elements (Fe and Ca) cannot justify such disorder, as similar differences in mass without any chemical variation usually modify the phonon characteristics, without inducing disorder. We can recognize disorder from the increase in the modes width and the reduction in its intensity. The variation of disorder with doping is depicted in Figure 6 for the stronger $\nu_1$ $PO_4$ mode at ~962 $cm^{-1}$ and both isotopic compounds. It can be observed that in FeHAp there is a continuous decrease in intensity and, at the same time, substantial increase in width with a characteristic change in behavior at $x \sim 0.2$ (Fig. 6a). On the other hand, FeDAp appears to become disordered faster, reaching the same asymptotic tendency at $x \sim 0.1$ (Fig. 6b). This behavior characterizes the other internal modes of the $PO_4$ tetrahedron, as shown in Figure 7. Again, in the FeHAp samples there is a slower continuous decrease in intensity than in FeDAp. Refinements of the XRD patterns for FeHAp and FeDAp revealed the same Fe content for same nominal x and therefore the differences in the disorder could not be due to differing amounts of Fe concentration in the two sample sets. The observed increased disorder is in agreement with the increased distortion index of the phosphate tetrahedron in the Fe-doped samples compared to the pure DAp. The distortion index was calculated from the P-O bond lengths found from the simultaneous Rietveld refinement of the X-ray and neutron diffraction patterns of the FeDAp sample series (Kyriacou et al. 2013). The obvious modification of the induced disorder by the deuteron substitution that affects the long-range order of the internal modes could be due to the additional processing (heat treatment at 600 °C during ion exchange of H with D) that would increase the disorder. In any case it is worthwhile to

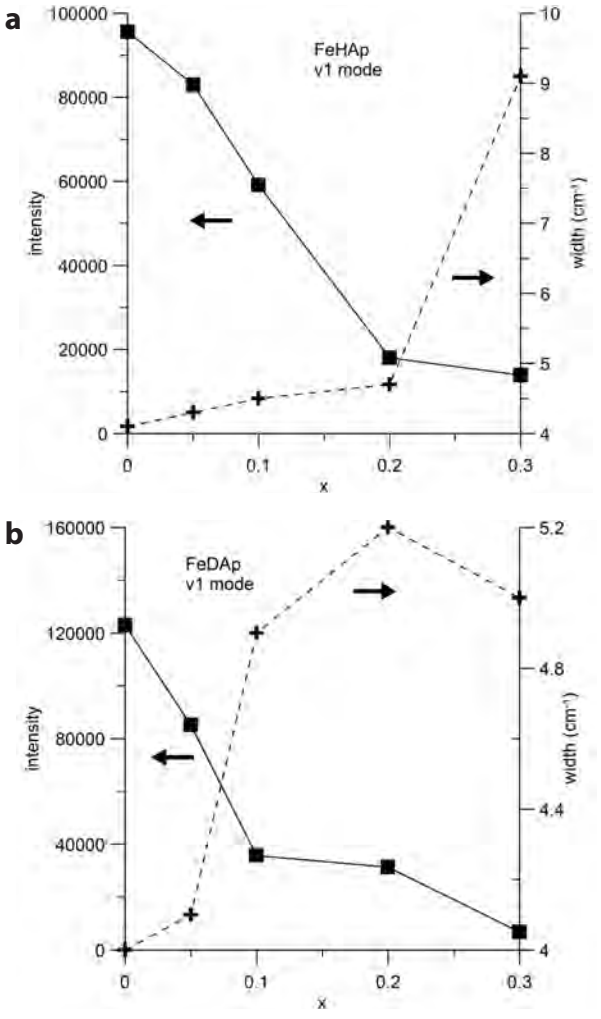


**FIGURE 6.** The dependence on Fe concentration of the intensity (squares, left axis) and width (crosses, right axis) of the $\nu_1$ mode of FeHAp (**a**) and FeDAp (**b**).

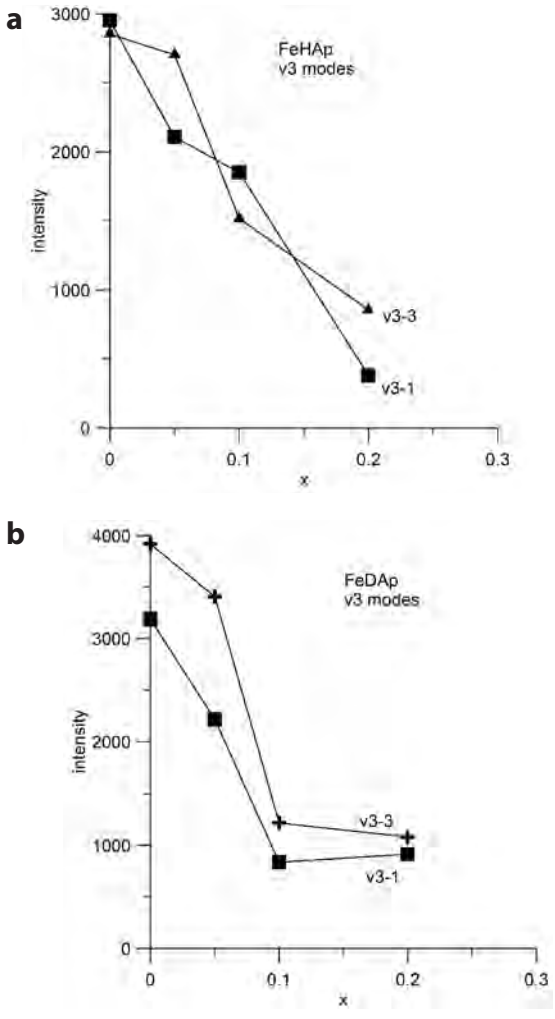


**FIGURE 7.** The dependence on Fe concentration of the intensity for two of the strong $\nu_3$ modes, $\nu_3$-1 (squares) at ~1027 cm$^{-1}$ and $\nu_3$-3 (crosses) at ~1046 cm$^{-1}$ of FeHAp (**a**) and FeDAp (**b**).

conduct further investigation since disorder may also mark an anharmonic phonon behavior.

In conclusion, we have studied by Raman and IR spectroscopy two sets of hydroxyapatite compounds with varying levels of atomic Fe substitution for Ca from 0 to 6%; one set of samples with H and the other deuterated. Only two modes were found to be affected by the deuteration, related to the OH group at ~3572 cm$^{-1}$ (internal stretching mode of OH) and ~631 cm$^{-1}$ (vibrational mode of $Ca_3$-OH). Iron substitution for Ca did not significantly affect the frequency of the modes, but damped the intensity of the internal modes substantially, whereby increasing their width. This is a clear indication of increased lattice disorder with increasing degree of Fe substitution. It was also found that HAp is less sensitive to disorder than the deuterated samples.

## IMPLICATIONS

Although Fe is a minor substituent for Ca in the structure of physiological hydroxyapatite, it affects their properties decidedly (Medeiros et al. 2002; De Vernejoul et al. 1984). Motivated by the disagreement on the lattice modifications induced by the Fe substitution, and a recent relevant study by combined XRD and neutron scattering on Fe- and deuteron-substituted hydroxyapatite (Kyriacou et al. 2013), we have carried out optical measurements on the same series of samples.

In this work, hematite has been detected even in samples with the smallest Fe concentration, which was below the detection limits of the XRD measurements, demonstrating the advantageous discrimination level of the Raman technique (Fig. 4). We have found that Fe substitution does not affect significantly the frequency of the strong modes that are related to internal vibrations of the $PO_4$ tetrahedra. On the contrary, the width and the intensity of those modes were found to be very sensitive to the structural disorder introduced by the Fe substitution. The disorder is related to the breaking of external bonds of the $PO_4$ tetrahedra, as previously found by XRD and neutron scattering (Kyriacou et al. 2013), and it is smaller in the hydroapatites compared to the deuterated ones. The FTIR measurements have revealed modes related to OH that challenge the results of ab initio calculations.

Our data provide substantial experimental evidence to test relative theories on the lattice effects of the Fe substitution.

## ACKNOWLEDGMENTS

Crystal structure and electron microscopy studies had been conducted at the Oak Ridge National Laboratory's High Flux Isotope Reactor and the Center for Nanophase Materials Sciences, sponsored by the Scientific User Facilities Division, Office of Basic Energy Sciences, U.S. Department of Energy. Preparation and characterization of the samples was supported by FAU's "Dissertation of the Year Award" to the third author.

## REFERENCES CITED

Antonakos, A., Liarokapis, E., and Leventouri, T. (2007) Micro-Raman and FTIR studies of synthetic and natural apatites. Biomaterials, 28, 3043–3054.

Calderin, L., Dunfield, D., and Stott, M. (2005) Shell-model study of the lattice dynamics of hydroxyapatite. Physical Review B, 72, 224304.

Cant, N.W., Bett, J.A.S., Wilson, G.R., and Hall, W.K. (1971) The vibrational spectrum of hydroxyl groups in hydroxyapatites. Spectrochimica Acta, 27A, 425–439.

Corno, M., Busco, C., Civalleri, B., and Ugliengo, P. (2006) Periodic ab initio study of structural and vibrational features of hexagonal hydroxyapatite $Ca_{10}(PO_4)_6(OH)_2$. Physical Chemistry Chemical Physics, 8, 2464–2472.

de Faria, D.L.A., Venancio Silva, S., and de Oliveira, M.T. (1997) Raman microspectroscopy of some iron oxides and oxyhydroxides. Journal of Raman Spectroscopy, 28, 873–878.

De Vernejoul, M.C., Pointillart, A., Golenzer, C.C., Morieux, C., Bielakoff, J., Modrowski, D., and Miravet, L. (1984), Effects of iron overload on bone remodeling in pigs. American Journal of Pathology, 116, 377–384.

Elliott, J.C. (1994) Structure and Chemistry of the Apatites and Other Calcium Orthophosphates. Elsevier.

Jiang, M., Terra, J., Rossi, A.M., Morales, M.A., Baggio Saitovich, E.M., and Ellis, D.E. (2002) $Fe^{2+}/Fe^{3+}$ substitution in hydroapatite: Theory and experiment. Physical Review B, 66, 224107.

Khudolozhkin, B.O., Urusov, V.S., and Kurash, V.V. (1974) Mössbauer study of the ordering of $Fe^{2+}$ in fluor-apatite structure. Geochemistry International, 11, 748–750.

Kyriacou, A., Leventouri, Th., Chakoumakos, B.C., Garlea, V.O., dela Cruz, C.B., Rondinone, A.J., and Sorge, K.D. (2013) Combined X-ray and neutron diffraction Rietveld refinement in iron-substituted nano-hydroxyapatite. Journal Materials Science, 48, 3535–3545. doi:10.1007/s10853-013-7148-5.

Leventouri, T., Bunaciu, C.E., and Perdikatsis, V. (2003) Neutron powder diffraction studies of silicon-substituted hydroxyapatite. Biomaterials, 24, 4205–4211.

Li, Y., Widodo, J., Lim, S., and Ooi, C.P. (2012) Synthesis and cytocompatibility of manganese (II) and iron (III) substituted hydroapatite nanoparticles. Journal Materials Science, 47, 754–763.

Low, H.R., Phothammachai, N., Maignan, A., Stewart, G.A., Bastow, T.J., Ma, L.L., and White, T.J. (2008) The crystal chemistry of ferric oxyhydroapatite. Inorganic Chemistry, 47, 11774–11782.

Martin, T.P., Merlin, R., Huffman, D.R., and Cardona, M. (1977) Resonant two magon Raman scattering in $Fe_2O_3$. Solid State Communications, 22, 565–567.

Massey, M.J., Baier, U., Merlin, R., and Weber, W.H. (1990) Effects of pressure and isotopic substitution on the raman spectrum of $\alpha$-$Fe_2O_3$: Identification of two-magnon scattering. Physical Review B, 41, 7822–7827.

McCarty, K.F. (1988) Inelastic scattering in $\alpha$-$Fe_2O_3$: Phonon vs magon scattering. Solid State Communications, 68, 799–802.

Medeiros, D.M., Plattner, A., Jennings, D., and Stoecker, B. (2002) Bone morphology, strength and density are compromised in iron-deficient rats and exacerbated by calcium restriction. Journal of Nutrition, 132, 3135–3141.

Morissay, R., Rodriguez-Lorenzo, L.M., and Gross, K.A. (2005) Influence of ferrous iron incorporation on the structure of hydroapatite. Journal Materials Science: Materials in Medicine, 16, 387–392.

Okazaki, M., and Takahashi, J. (1997) Heterogeneous iron-containing fluoridated apatites. Biomaterials, 18, 11–14.

Park, E., Condrate, R.A. Sr., Lee, D., Kociba, K., Gallagher, P.K. (2002) Characterization of hydroxyapatite: before and after plasma spraying. Journal Materials Science; Materials in Medicine, 13, 211–218.

Pedone, A., Corno, M., Civalleri, B., Malavasi, G., Menziani, M.C., Segre, U., and Ugliero, P. (2007) An ab initio parametrization interatomic force field for hydroxyapatite. Journal of Materials Chemistry, 17, 2061–2068.

Penel, G., Leroy, P.G., Rey, C., and Bres, E. (1998) Micro-Raman spectral study of the $PO_4$ and $CO_3$ vibrational modes in synthetic and biological apatites. Calcified Tissue International, 63, 475–481.

Salviulo, G., Bettinelli, M., Russo, U., Speghini, A., and Nodari, L. (2011) Synthesis and structural characterization of $Fe^{3+}$-doped calcium hydroxyapatite: role of precursors and synthesis method. Journal Materials Science, 46, 910–922.

Shim, S.H., and Duffy, T.S. (2001) Raman spectroscopy of $Fe_2O_3$ to 62 GPa. American Mineralogist, 87, 318–326.

Srivastava, G.P. (1990) The Physics of Phonons. Taylor and Francis.

Ulian, G., Valdrè, G., Corno, M., and Ugliero, P. (2013) The vibrational features of hydroxyapatite and type A carbonated apatite: A first principle contribution. American Mineralogist, 98, 752–759.

Vignoles-Montrejaud, M. (1984) Contibution a L'etude des Apatites Carbonate es de Type B. These d'Etat, Institut National Polytechnique de Toulouse.

Wang, J., White, W.B., and Adair, J.H. (2005) Optical properties of hydrothermally synthesized hematite particulate pigments. Journal of the American Ceramic Society, 88, 3449–3454.

Wopenka, B., and Pasteris, J.D. (2005) A mineralogical perspective on the apatite bone. Materials Science and Engineering C, 25, 131–143.

Wu, H.C., Wang, T.W., Sun, J.S., Wang, W.H., and Lin, F.H. (2007) A novel biomagnetic nanoparticle based on hydroapatite. Nanotechnology, 18, 165601–165609.

MANUSCRIPT RECEIVED JUNE 17, 2016
MANUSCRIPT ACCEPTED AUGUST 29, 2016
MANUSCRIPT HANDLED BY DANIEL HARLOV